Graded calcium spikes differentially signal neurotransmitter input in cerebrospinal fluid contacting neurons of mouse spinal cord

Emily Johnson, Marilyn Clark, Claudia MacLean, Jim Deuchars, *Susan A. Deuchars, *Jamie Johnston

School of Biomedical Sciences, Faculty of Biological Sciences, University of Leeds, Leeds, LS2 9JT

*Corresponding Author

Susan A. Deuchars: S.A.Deuchars@leeds.ac.uk
Jamie Johnston: j.johnston@leeds.ac.uk

Abstract

The action potential and its all-or-none nature is fundamental to neural communication. Canonically the action potential is initiated once voltage-gated Na^+ (Na_V) channels are activated and their rapid kinetics of activation and inactivation give rise to the all-or-none nature. Here we show that cerebrospinal fluid contacting neurons (CSFcNs) surrounding the central canal of the mouse spinal cord employ a different strategy. Rather than using Nav channels to generate binary spikes, CSFcNs use two different types of voltage-gated Ca^{2+} channel, enabling spikes of different amplitude. T-type Ca^{2+} channels are required for spontaneous spiking and generate lower amplitude spikes, whereas large amplitude spikes require high voltage activated Cd^{2+} sensitive Ca^{2+} channels. We show that these different amplitude spikes signal input from different transmitter systems; purinergic inputs evoke smaller T-type dependent spikes while cholinergic inputs evoke large T-type independent spikes. Different synaptic inputs to CSFcNs can therefore be signalled by the spike amplitude.

Introduction

Cerebrospinal fluid contacting neurons (CSFcNs) surround the central canal of the spinal cord and project a single dendritic like structure into the CSF through the ependymal cells that form the border of the central canal (Djenoune et al., 2014). Upon their identification it was suggested that CSFcNs form a sensory "sagittal organ" within the spinal cord (Kolmer, 1921). Subsequent studies in zebrafish have indicated that different CSFcN populations exhibit fast calcium responses to bending of the spinal cord and synapse onto distinct motor neuron populations and afferent interneurons to regulate motor behaviour. In these studies, disruption of CSFcN signalling leads to impairment of postural control (Hubbard et al., 2016), spinal morphogenesis (Sternberg et al., 2018) and locomotion (Bohm et al., 2016, Fidelin et al., 2015, Hubbard et al., 2016, Wyart et al., 2009). Recordings from lamprey also indicate that CSFcNs play a homeostatic role in locomotion; CSFcNs were sensitive to pH and deviations from normal pH reduced locomotor output (Jalalvand et al., 2016a, Jalalvand et al., 2016b, Jalalvand et al., 2014). These findings indicate a key role for CSFcNs in spinal sensory signalling in lower vertebrates yet little is known about the function or indeed the signalling mechanisms of these cells in mammalian systems.

Voltage gated Na^+ (Na_V) channels are widely considered to be fundamental for neuronal excitability and a requirement for the generation and propagation of action potentials throughout the central and peripheral nervous systems (Wang et al., 2017). Whilst this assumption holds true in the majority of mammalian neurons, sensory systems commonly utilise Ca^{2+} as the primary mediator of electrogenesis. Within auditory hair cells $Ca_V1.3$ (L-type) channels mediate spikes and glutamate release (Brandt et al., 2003, Zampini et al., 2010). Similarly, retinal bipolar cells rely on low-voltage activated (T-type) Ca^{2+} channels to initiate regenerative potentials and spiking activity (Dreosti et al., 2011, Hu et al., 2009). As Ca_V channels operate over a wide range of membrane potentials and facilitate both spiking and graded events, their prevalence enables sensory neurons to respond to a wide range of inputs (Lipin and Vigh, 2015). Such a mechanism for signalling would also be advantageous for CSFcNs if they fulfil a sensory role. Single-cell RNA sequencing indicates that mouse spinal CSFcNs abundantly express mRNA for all 3 isoforms of T-type calcium channel (Ca_V3-1, -2, -3) and numerous HVA channels, including $Ca_V1.3$ (Rosenberg et al., 2018) an L-type channel predominantly expressed by sensory neurons and neurosecretory cells (Comunanza et al., 2010, Joiner and Lee, 2015).

CSFcNs have been described in a host of mammalian species ranging from mice to primates (Djenoune et al., 2014) including humans (Humphrey, 1947). Uniquely (within the CNS) express polycystic kidney disease 2-like 1 protein (PKD2L1) (Djenoune et al., 2014, Huang et al., 2006). Due to the lack of in vivo mammalian studies, it is not clear whether the function of CSFcNs is conserved between amniotes and mammals. To begin addressing whether

CSFcNs constitute a novel sensory system within the adult mammalian spinal cord we used 2-Photon Ca^{2+} imaging to study the activity of mouse CSFcNs. Our findings reveal that adult mouse spinal CSFcNs exhibit T-type Ca^{2+}channel dependent spontaneous activity and, in parallel to other sensory systems, employ Ca_V channels to generate spikes of graded amplitudes to differentially respond to activation of different neurotransmitter receptors.

Results

The VGAT promotor drives expression in all PKD2L1 positive CSFcNs

To enable imaging of neural activity within CSFcN populations, we targeted GCaMP6f to CSFcNs of the central canal by driving its expression under the VGAT promotor. Within the spinal central canal GCaMP6f was expressed by cells with stereotypical CSFcN morphology, displaying a single bulbous apical process extending into the lumen of the central canal (Fig 1A). Polycystic kidney disease 2-like 1 protein (PKD2L1), the canonical marker of CSFcNs (Djenoune et al., 2014), displayed 100% overlap with these GCaMP6f positive cells (n= 206 cells, 3 mice, Fig 1). These data indicate that GCaMP6f is expressed in the entire population of CSFcNs in our VGAT-GCaMP6f mice and we took advantage of 2-photon microscopy to image their activity in acute spinal cord slices.

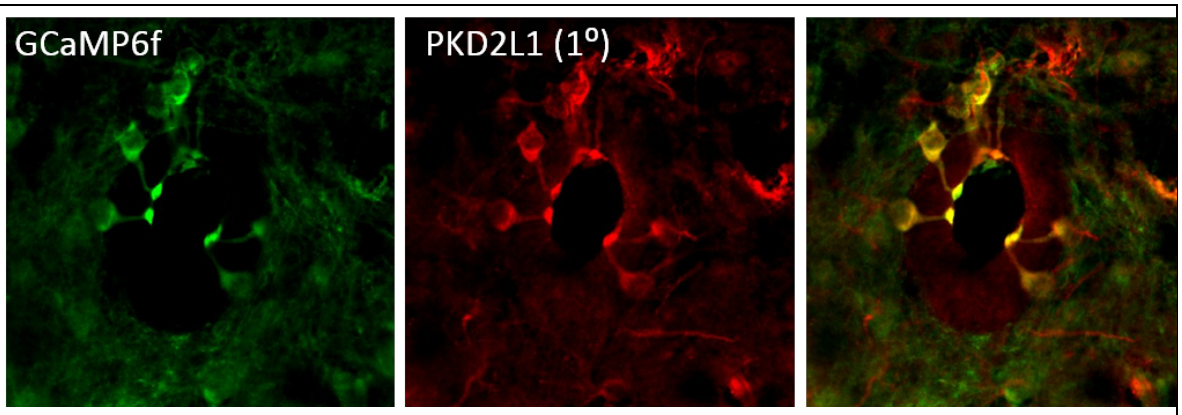

Figure 1 – VGAT promotor successfully drives GCaMP6f expression in CSFcNs. Images showing how expression of GCaMP6f (green, **left**) and polycystic kidney disease 2-like 1 protein (red, **centre**) colocalised (merged, **right**) around the central canal.

CSFcNs generate variable amplitude spikes

We observed widespread spontaneous activity across the population of CSFcNs (Fig 2A,B) similar to that reported from *in vivo* Ca^{2+} imaging in the larval zebrafish (Sternberg et al., 2018). We detected Ca^{2+} spikes using their first derivative (Fig. 2C) which enabled separation of summated spikes. Spontaneous activity occurred at a low frequency in CSFcNs; across a population of 61 CSFcNs the mean firing rate was 0.16 Hz (IQR = 0.12 - 0.23 Hz, Fig. 2G). This spontaneous activity is likely governed by a simple Poisson process as the distributions

of inter-spike-intervals decayed exponentially (Fig. 2 D) and had coefficients of variation close to 1 (Fig. 2H). No differences were observed between slices prepared from juvenile (P14-P24) or adult mice (P36-P47) (Fig 2G & H). Strikingly, the spikes in individual CSFcNs were of variable amplitude with distinct low and high amplitude events detected (Fig. 2 B, C & F) and correspondingly had multi-modal amplitude distributions (Fig 2 E & I). The larger amplitude spikes may simply reflect multiple underlying action potentials with an interval too short for us to resolve the separate spikes. The probability of this occurring can be determined from the following equation:

$$P(k\ spikes\ in\ interval\ t) = \frac{(rt)^k e^{-(rt)}}{k!}$$

Where *k* is the number of spikes, *t* is the minimal spike interval that we observed of 0.12 s and *r* is the mean rate of firing. For the two example cells in Fig. 2, the probabilities were 1.387×10^{-4} and 6.696×10^{-5} for the grey and blue cells respectively. These probabilities predict that fewer than one such multi-action potential spike would be expected during the 850 s recording in Fig. 2B, yet for both cells we detected ≥27 large amplitude spikes (Fig. 2E & F). This led us to explore the ionic mechanisms underlying these multi-amplitude calcium spikes in CSFcNs.

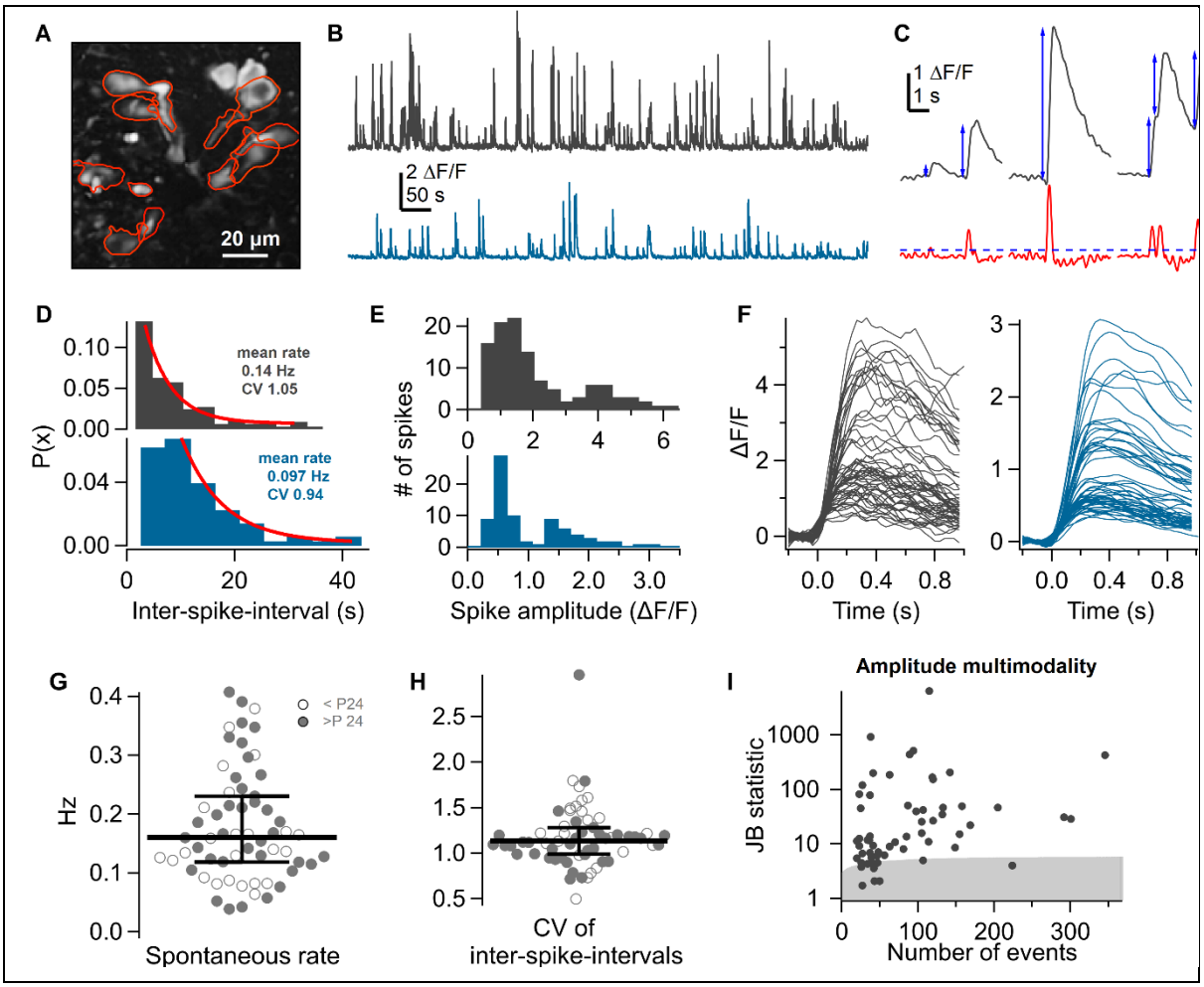

Figure 2 - CSFcNs fire spontaneously at low rates with variable amplitudes

A) Correlation image showing the segmented CSFcNs in the field of view. **B)** Spontaneous activity of 2 CSFcNs from A. **C)** Events were detected on the differentiated trace (red) with an automatically determined threshold (see methods), blue arrows indicate amplitude measurements. **D)** Distributions of the inter-spike-intervals for the 2 cells in B, red fits are single exponentials indicating a Poisson process. **E)** Spike amplitude histograms for the two CSFcNs in B were multimodal. **F)** Aligned events show different spike amplitudes despite similar time courses (events occurring in close proximity have been removed for clarity). **G)** Spontaneous rate across 54 CSFcNs (n=7) was 0.162 Hz (median with IQR 0.121-0.220 Hz). No difference between juvenile (open circles) and adult (filled circles). **H)** The coefficient of variation of the inter-spike-intervals across the population was 1.13 (median with IQR 0.95-1.22) No difference between juvenile (open circles) and adult (filled circles). **I)** The spike amplitudes within each cell was not normally distributed in 50 of 61 cells, grey shaded area shows critical value of the Jarque-Bera (JB) statistic, see methods.

T-Type Ca^{2+} channels are required for spontaneous activity in CSFcNs

The spontaneous activity of CSFcNs was unaffected by bath application of the voltage-gated sodium channel blocker tetrodotoxin (TTx, 1µM, Fig 3). This was unexpected since mRNA for Na_V1.-1,-3,-6,-7 has been detected in CSFcNs (Rosenberg et al., 2018), all of which are TTx sensitive (Lee and Ruben, 2008), but these do not appear to contribute to the frequency of CSFcN Ca^{2+} events (n=33 cells, Fig 3C). The amplitude of spontaneous events was also unaffected by TTx (Fig 3B), indicating that Nav dependent spikes do not play an important role in the soma and apical dendrite.

We have previously shown that CSFcNs exhibit action potentials in response to current injection or to activation of cholinergic receptors (Corns et al., 2015). Though these action potentials were slower and of lower amplitude than typical Na_V-dependent action potentials. Other sensory neurons transmit information using Ca_V spikes in place of Na_V spikes (Baden et al., 2011, Dreosti et al., 2011, Hu et al., 2009, Zampini et al., 2010), so we next tested whether the spontaneous activity in CSFcNs was Ca_V-dependent (Fig 4). Bath application of the broad spectrum high voltage activated (HVA) Ca_V channel blocker cadmium (Cd^{2+}, 100µM) significantly reduced the frequency (Fig 4B) and amplitude (Fig 4C) of spontaneous Ca^{2+} events in CSFcNs (to 56 and 54% of control respectively, n=31 cells), although low amplitude events persisted in the majority (30 out of 31) of CSFcNs (Fig 4A-C). Cd^{2+} at 100µM effectively blocks all HVA Ca_V channels, but has negligible effects on low voltage activated (LVA, T-type) Ca_V channels (Huang, 1989). Consistent with this idea, we found that Cd^{2+} changed the event

amplitude histograms from multi-modal to unimodal, selectively attenuating the larger amplitude events (Fig 4D,E). This indicates that T-type Ca^{2+} channels may be responsible for

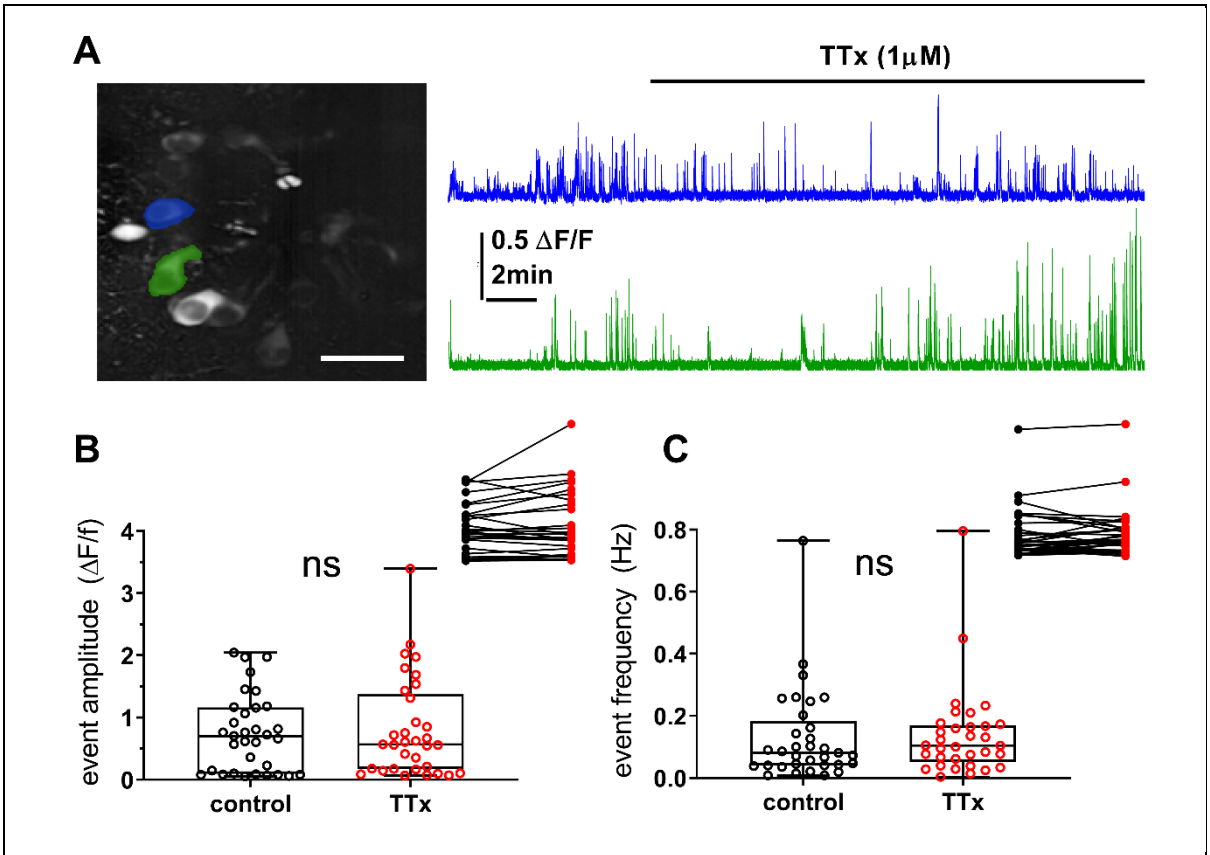

Figure 3 – TTx has no effect on spontaneous Ca^{2+} events

A, (*left)* correlation image showing 2 example segmented CSFcNs (scale bar 30μm) with ***(right)*** corresponding traces showing lack of effect of TTx (1μM, black bar). **B-C,** TTx (red symbols) is without effect on spontaneous Ca^{2+} event amplitude **(B)** or frequency **(C)** (n=33 CSFcNs (3 slices), N=3 animals, Wilcoxon test, p=0.2011 and p=0.396 respectively)

the majority of events and a proportion of these reach the threshold to trigger opening of HVA Ca^{2+} channels, thus boosting the amplitude of the events.

Indeed, we found that T-type Ca^{2+} channels play a major role in the spontaneous activity in CSFcNs: bath application of the selective T-type blocker ML218 (3μM in 0.01% DMSO) dramatically reduced the frequency of Ca^{2+} events in all CSFcNs (to 10% of control, n=27 cells) with complete inhibition observed in 20 of 27 spontaneously active CSFcNs (Fig4F-G). DMSO alone caused a small but significant reduction in the frequency of spontaneous activity of CSFcNs (62% of control, n=25 cells) but was without effect on event amplitude. Collectively these results show that CSFcNs lack Na_V-dependent activity (Fig. 3A) but instead can generate Ca_V-dependent spikes of variable amplitudes (Fig. 2), with the majority of

spontaneous events requiring T-type channels (Fig. 4F-G) and larger amplitude events also involving HVA channels (Fig 4A-E).

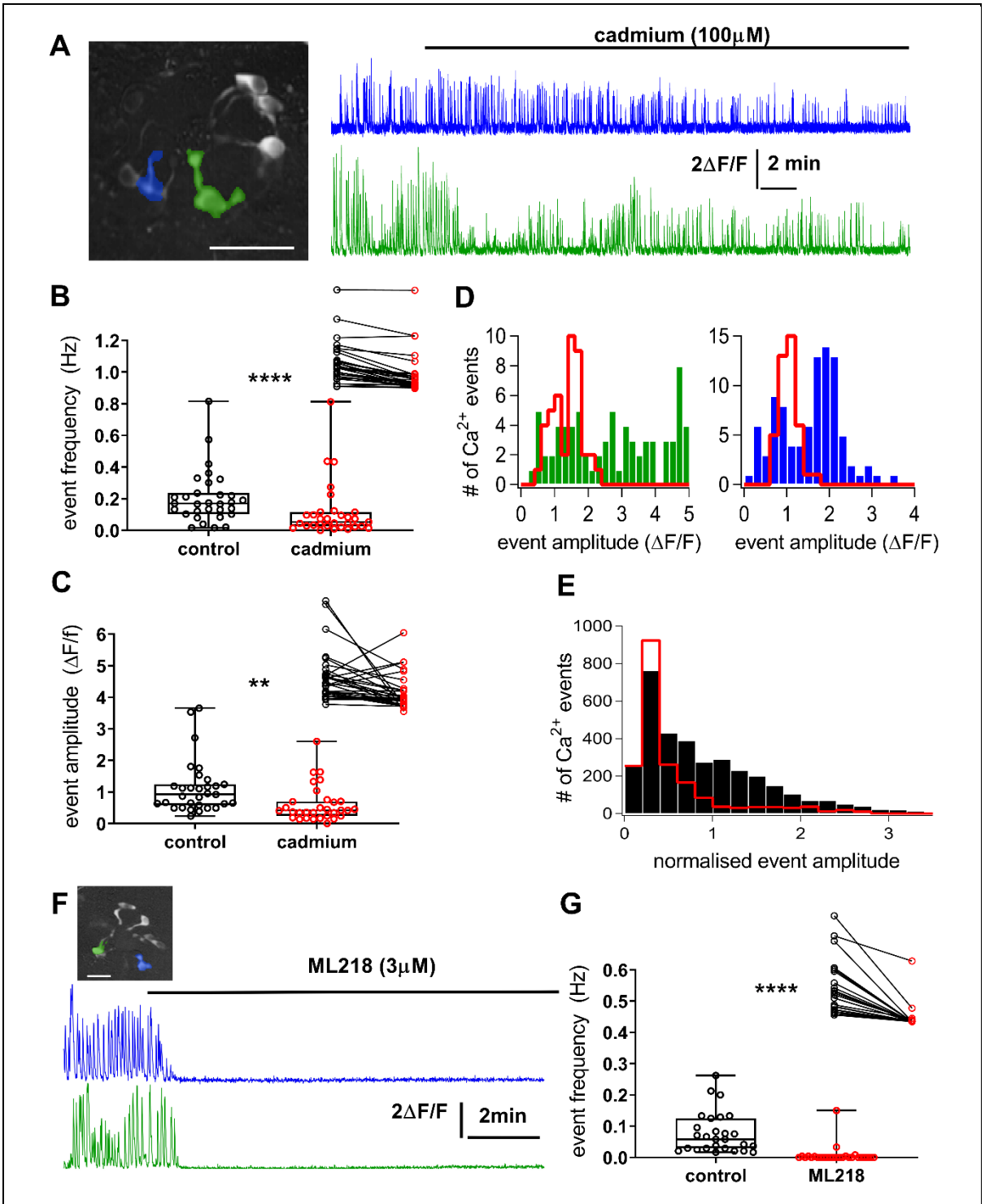

Figure 4 – Voltage gated Ca^{2+} channels mediate spontaneous Ca^{2+} events

A ***(left)*** correlation image showing example segmented CSFcNs (scale bar 30µm) with ***(right)*** corresponding traces showing the effects of **(A)** cadmium (Cd, 100µM). **B-C,** Cd (red symbols) significantly reduces the frequency **(B)** and amplitude **(C)** of spontaneous Ca^{2+} events, insets - effects of Cd on individual CSFcNs, (n=31 CSFcNs, 4 slices, N=2 animals,

Wilcoxon test, p=>0.0001 and p=0.0012 respectively). **D,** event amplitude histograms (from the 2 example CSFcNs in A) and **E,** normalised histogram of all CSFcNs (each event divided by average amplitude in control condition, n=31 CSFcNs), both showing that Cd (red line) selectively reduces high amplitude Ca^{2+} events. **F (inset*)*** correlation image showing example segmented CSFcNs (scale bar 30µm) with corresponding traces showing the effects of ML218 (3µM). **G,** ML218 significantly reduces the frequency of spontaneous Ca^{2+} events (n=27 cells (4 slices), N=4 animals, Wilcoxon test, p=>0.0001).

Depolarisation evoked activity in CSFcNs is mediated by voltage gated Ca^{2+} channels

We have demonstrated that T-Type Ca^{2+} channels are the major contributor to spontaneous activity, but do they also govern evoked activity? To directly test this, we evoked depolarisations in the entire population of CSFcNs by focal ejection of 40 mM K^+ within the central canal. This depolarising stimulus reliably elicited Ca^{2+} spikes within all CSFcNs including those previously silent (Fig 5A). This enabled us to calculate that across 190 CSFcNs, 70% were spontaneously active and the amplitude of K^+ evoked Ca^{2+} spikes was significantly larger in the spontaneously active cells (Fig 5B). The dorso-ventral positioning of spontaneous vs silent CSFcNs around the central canal was similar (Fig 5C), indicating that there were no specific subgroups of spontaneously active CSFcNs clustering in specific poles of the central canal. Standard aCSF focally ejected in place of high K^+ did not evoke activity (data not shown), indicating no contribution from mechanosensitive channels at the pressures used. Bath application of Cd^{2+} or ML218 significantly reduced the amplitude of K^+-evoked Ca^{2+} events to 30% (Fig 5D,F) and 25% (Fig 5E,F) of control respectively. K^+-evoked Ca^{2+} events appeared to involve both HVA and T-type channels in combination as neither of the antagonists abolished the depolarisation evoked spikes. Together these data imply that CSFcNs can generate variable amplitude spikes due to differing thresholds of the underlying Ca^{2+} channels; T-type channels generate smaller amplitude spikes and with strong enough stimulation HVA Ca^{2+} channels are recruited to generate larger spikes. We next explored whether this mechanism could be used to distinguish between different synaptic inputs.

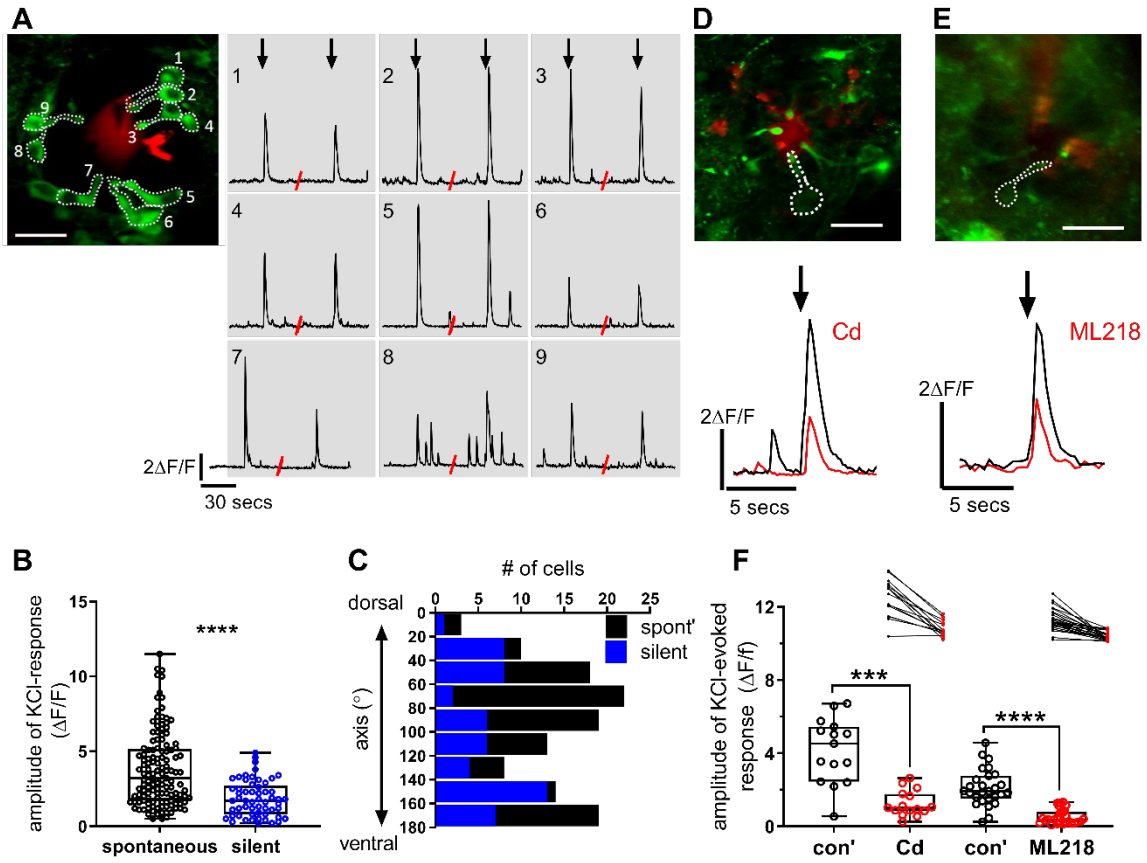

Figure 5 – Voltage gated Ca^{2+} channels mediate depolarisation-evoked Ca^{2+} events

A, (*left)* projection image showing 9 CSFcNs within a field of view (green, white lines highlighting manually identified ROIs, scale bar 30µm) and SR101 ejected from puff electrode in central canal (CC, red): (***right)*** example traces for each CSFcN showing how Ca^{2+} events are consistently evoked by focal application of K^+ (40mM, 200ms, black arrows, red lines denote 120sec time-break in recording). **B,** amplitude of K^+-evoked Ca^{2+} events is significantly larger in spontaneously active (black symbols, n=133) compared to non-spontaneously active (silent, blue symbols, n=57) CSFcNs (n=22 slices, N=9 animals, Mann-Whitney test, p= >0.0001). **C,** the locations of spontaneous (n=126 CSFcNs, black bars) and silent (n=126 CSFcNs, n=55 CSFcNs, blue bars) CSFcNs along the dorsoventral axis of the central canal are similar (n=20 slices, N=8 animals). **D,E, *(top)*** example CSFcN (white line, scale bar 30µm) and ***(bottom)*** corresponding example trace recorded in control (black traces) and **(D)** cadmium (100µM) or **(E)** ML218 (3µM) conditions (red traces). **F,** amplitude of K^+-evoked Ca^{2+} events is significantly reduced by Cd (n=15 CSFcNs (2 slices), N=1 animal, Wilcoxon test, p=0.0001) and ML218 (n=27 CSFcNs (4 slices), N=3 animals, Wilcoxon test, p= <0.0001).

T-type Ca^{2+} channels boost weak inputs to CSFcNs

Low-voltage activated T-type Ca^{2+} channels can amplify smaller synaptic inputs by opening in response to EPSPs (Ly et al., 2016) or indeed IPSCs (Boehme et al., 2011, Lattanzi et al., 2020). To test whether T-type channels are serving a similar function in CSFcNs, we stimulated with two different neurotransmitters, acetylcholine (ACh) and ATP, which generated responses with significantly different amplitudes (Fig 6C). Focally applied ACh (1mM) evoked large Ca^{2+} spikes in all CSFcNs (100% of 67 CSFcNs examined) which were significantly antagonised by the nicotinic antagonist mecamylamine (MCA, 50μM, to 28% of control). In contrast, focally applied ATP (300μM) evoked smaller responses (Fig. 6C) and failed to evoke any response in 24 of 83 cells. There was also a marked difference in the effect of T-type channel inhibition; ACh responses were unaffected by ML218 whereas (Fig. 6 A & D), whereas ATP responses were significantly attenuated (92.5% inhibition, Fig. 6 B & E). These data are consistent with the idea that weaker ATP inputs are amplified by T-type channels into a small amplitude spike, whereas the stronger ACh inputs directly recruit the higher threshold HVA channels.

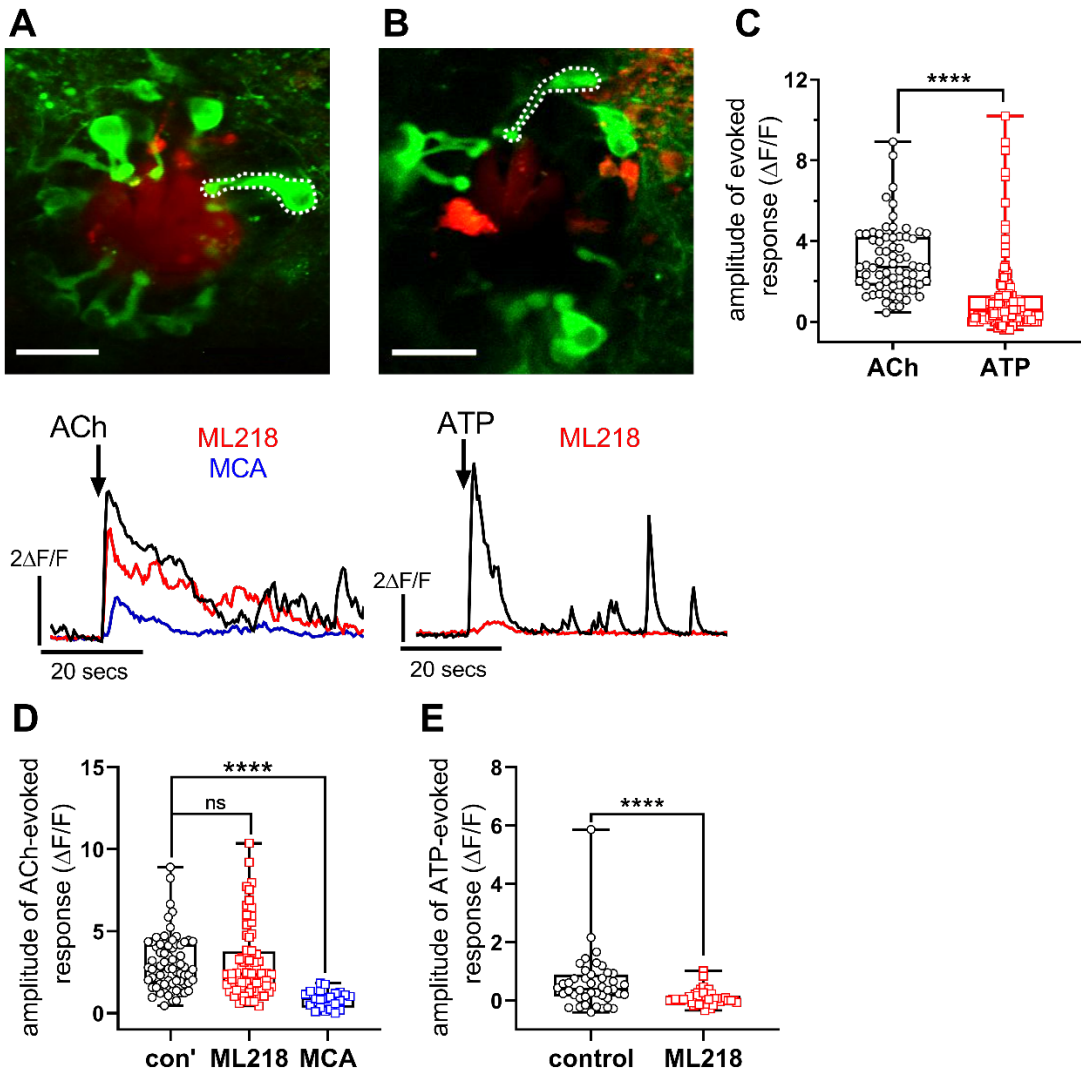

Figure 6 – T-type Ca^{2+} channels boost weak inputs to CSFcNs

A,C, (top) projection image showing example segmented CSFcNs (scale bar 30µm) with ***(bottom)*** corresponding traces showing the effects of ML218 (3µM, red traces) on control Ca^{2+} responses (black traces) following focal application of: **(A)** ACh (1mM, 200ms) also with mecamylamine (MCA, 50µM, blue trace), or **(B)** ATP (300µM). **C,** the amplitude of ACh-evoked Ca^{2+} events (n=68 CSFcNs) is significantly larger than ATP-evoked Ca^{2+} events (n=138 CSFcNs, Mann-Whitney test, p=>0.0001). **D,** amplitude of ACh-evoked Ca^{2+} responses are significantly reduced by MCA (50µM, blue symbols, n=22 CSFcNs (2 slices), N=1 animal), but not ML218 (3µM, red symbols, n=68 CSFcNs (7 slices), N=3 animals), (Kruskal-Wallis test, p=<0.0001 and p=>0.9999 respectively). **E,** amplitude of ATP-evoked Ca^{2+} responses are significantly reduced by ML218 (n=43 CSFcNs, (9 slices) N=4 animals, Wilcoxon test, p=<0.0001).

Functional P2X and P2Y expression in CSFcNs

We confirmed that ATP was acting on purinergic receptors using the broad spectrum P2X antagonist PPADs. The amplitude of ATP evoked Ca^{2+} spikes was attenuated by 65% in 12 of 15 CSFcN with application of PPADS (Fig 7A & B). The $P2X_3$ specific antagonist A317 significantly antagonised ATP-evoked responses in ventral, but not dorsal CSFcNs (Fig 7C,D). A weak negative correlation (R^2 = 0.21, P = 0.0484) between the extent of antagonism and DV location was apparent for A317, but not for PPADs (data not shown). These findings indicate that ATP is indeed acting in part through P2X receptors and that P2X3 receptors are the main contributor in ventral CSFcNs. In addition to P2X, ATP can also act on metabotropic P2Y receptors (Jacobson et al., 2009) which may explain the incomplete inhibition observed with PPADs (Fig 7B). We tested for a contribution of P2Y receptors using the P2Y agonist UTP and found clear Ca^{2+} spikes in 22 of 40 CSFcNs tested and these were completely inhibited by T-type channel antagonism (ML218, 3μM n=17 CSFcNs, Fig 7E,F). Furthermore, in 13 CSFcNs we saw small decreases in Ca^{2+} fluorescence with ATP which were immediately followed by a large Ca^{2+} spike (Fig 7G). In these cells ML218 did not alter the initial Ca^{2+} decrease but abolished the subsequent Ca^{2+} spike (Fig 7H). Such bidirectional responses were never observed with ACh or K^+ stimulation.

Together these data indicate that a subset of CSFcNs are sensitive to ATP which is mediated through both P2X (Fig 7A-D) and P2Y receptors (Fig 7E), but crucially T-type channels are required to convert activation of these receptors into spikes (Figs. 6C-F & 7E-H). This was in contrast to ACh (Fig 6A-B) and K^+ evoked responses (Fig. 5) which were strong enough to recruit HVA Ca^{2+} channels. Indeed the amplitudes of ATP evoked spikes were significantly smaller than those of ACh (Fig 6C). In these intriguing neurons, spikes appear to operate in a graded rather than all-or-none fashion. In conclusion we show that CSFcNs can signal with different amplitudes depending on the strength of their input.

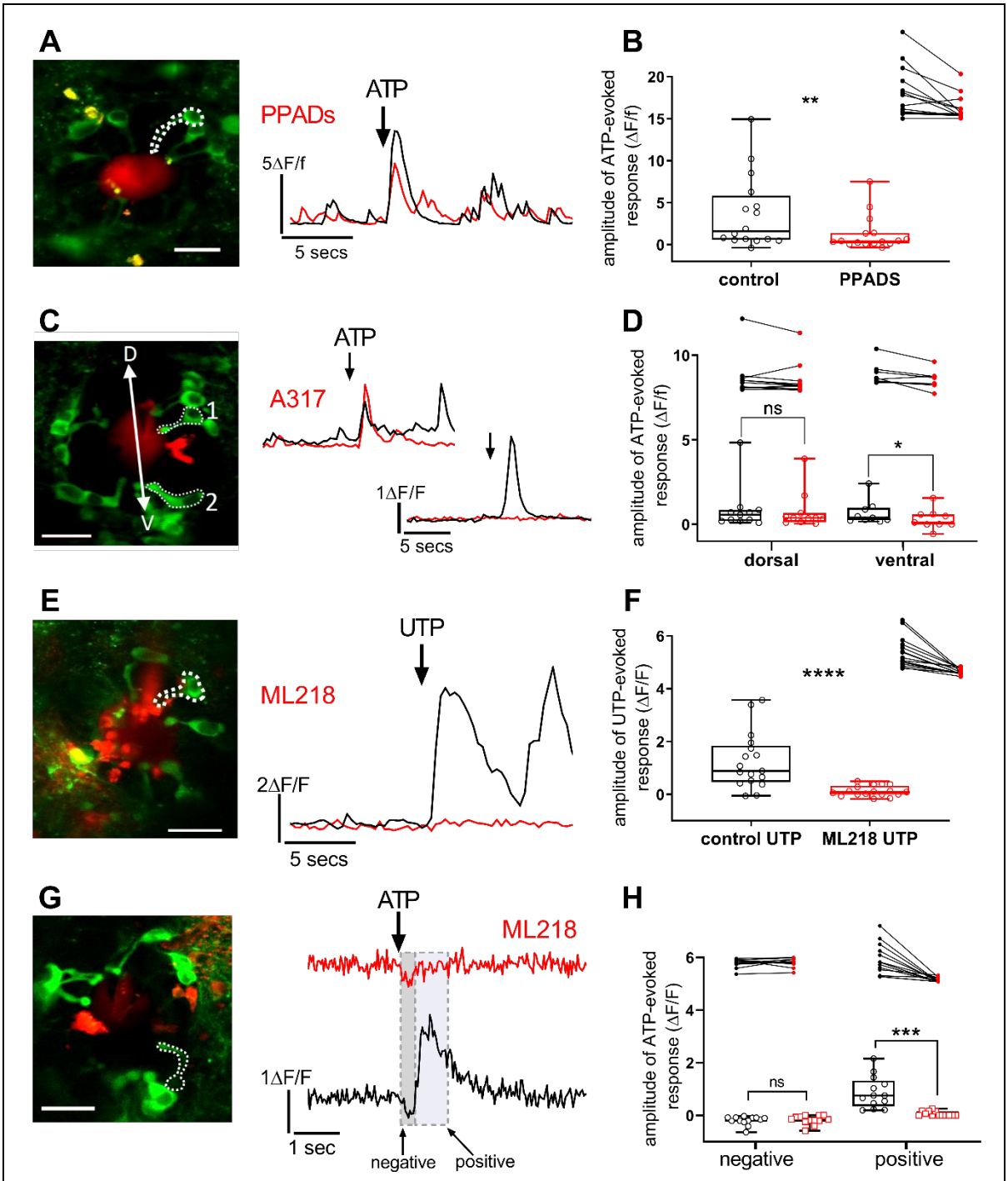

Figure 7 –Multiple types of purinergic inputs to CSFcNs

A,C,E,G, (*left)* projection image showing example segmented CSFcNs (scale bar 30μm) with ***(right)*** corresponding traces showing the effects of **(A)** PPADs (10μM), **(B)** A317 (1μM) and **(E,G)** ML218 (3μM), (red traces) on control Ca^{2+} responses (black traces) following focal application of **(A,C,G)** ATP or **(E)** UTP (both 300μM, 200ms, black arrows). **B,** the amplitude of ATP-evoked Ca^{2+} events is significantly reduced by PPADs (red symbols, n=15 CSFcNs (4 slices), N=2 animals, Wilcoxon test, p=0.0013), inset showing effects of PPADs on individual CSFcNs. **C,** A317-mediated antagonism occurs only in ventral, not dorsal, CSFcNs, (red symbols, 3 slices, N=2 animals, *dorsal* n=11 CSFcNs, p=0.1748, *ventral* n=9

CSFcNs, Wilcoxon test, p=0.0117), insets showing effects of A317 on individual CSFcNs. **F,** amplitude of UTP-evoked Ca^{2+} events is significantly reduced by ML218 (red symbols, n=17 CSFcNs (3 slices, N=2 animals, Wilcoxon test, p=>0.0001). **G,** ***(right)*** some ATP-evoked Ca^{2+} responses in control conditions (black line) are bipolar: i.e. made up of an initial Ca^{2+} decrease (negative) followed by a rebound Ca^{2+} increase (positive). **H,** ML218 selectively antagonises the positive, but not the negative, component of bipolar ATP-evoked Ca^{2+} responses (red symbols, n=13 CSFcNs, (9 slices) N=4 animals, Wilcoxon tests, negative p=0.4038, positive p=0.0002).

Discussion

The spike, or action potential, and its "all-or-none" nature is thought to be a fundamental quantum of neural processing. We show that rather than the typical Na_V channels, CSFcNs in the spinal cord of young and adult mice use Ca_V channels to generate spikes and that by employing different types of Ca_V channel they are able to generate graded spikes of variable amplitude. CSFcNs are able to use these graded spikes to differentially signal which neurotransmitter system is providing their input.

Na^+ dependent spikes are the ubiquitous mechanism for action potential generation throughout the mammalian brain (Raghavan et al., 2019), whilst Ca^{2+} spikes are typically utilised for dendritic signal integration (Golding et al., 1999, Major et al., 2013, Tran-Van-Minh et al., 2016, Xu et al., 2012). We find that, in contrast, CSFcNs employ Ca^{2+} spikes in their endbulb and soma. Whilst this does not preclude a role for Na^+ spikes in the axons of CSFcNs, which project to the ventral fissure (Stoeckel et al., 2003), it suggest that they are absent or at low densities in the soma and endbulb. In close parallel, somatic Ca^{2+} spikes are a prominent feature of various other sensory cells including retinal bipolar cells (Baden et al., 2013a) and auditory hair cells (Marcotti et al., 2003). Retinal bipolar cells signal with graded analogue signals as well as spikes (Dreosti et al., 2011), both of which are mediated by Ca_V channels (Baden et al., 2013, Hu et al., 2009). Such variations in the amplitudes of Ca^{2+} signals likely support the multivesicular amplitude code used by these synapses (James et al., 2019). Both T-type and L-type Ca^{2+} channels contribute to spiking in retinal bipolar cells (Hu et al., 2009) and in a direct parallel with our findings, T-type channels are required for spontaneous firing while L-type channels influence the shape and duration of Ca^{2+} events (Ma and Pan, 2003).

Inner hair cells (IHCs) can signal with graded and spiking responses predominantly through Ca_V channels (Marcotti et al., 2003, Johnson et al., 2011) and spontaneous Ca^{2+}-mediated APs in IHCs are intrinsically generated and are influenced by both ACh and ATP (Johnson et al., 2011). Since their identification, CSF-CNs have been proposed to be sensory neurons (Kolmer, 1921) and more recent work has demonstrated their functional role in both mechano- and chemo- sensation (Bohm et al., 2016, Fidelin et al., 2015, Hubbard et al., 2016, Jalalvand et al., 2018). It seems then that the adoption of Ca^{2+} spikes to enable variable amplitude Ca^{2+} events is a common feature of neurons across different sensory systems.

The functional role of CSFcNs in the mammalian spinal cord is yet to be determined, however they are recipients of numerous axon terminals on their basal pole; including purinergic and cholinergic inputs (Stoeckel et al., 2003; Alfaro-Cervello et al., 2012; Corns et al., 2015). We show that inputs from such purinergic and cholinergic receptors are processed differently by CSFcNs; purinergic input is weaker evoking smaller amplitude T-type dependent spikes whereas cholinergic inputs evoke larger spikes that do not depend on T-type channels (Fig 6).

A pertinent question is what is the role of these different amplitude spikes in CSFcNs? The apical process within the lumen of the central canal contains vesicles (Jaeger et al., 1983; Alfaro-Cervello et al., 2012) and may release GABA and other substances from this site. CSFcNs also send an axon to the ventromedial fissure where their synaptic terminals intermingle with axons of the corticospinal tract (Stoeckel et al., 2003). How might the different spike types we describe contribute to transmitter release? Typically, the HVA P/Q and N-type Ca^{2+} channels are coupled to transmitter release in neural cells. However, numerous examples of T-type Ca^{2+} channel activity governing transmitter release exist, including in: neuroendocrine cells in the pituitary (Tomic et al., 1999), adrenal glands (Mlinar et al., 1993, Schrier et al., 2001), retinal bipolar cells (Pan et al., 2001) and olfactory bulb neurons (Fekete et al., 2014). It is therefore possible that the smaller T-type Ca^{2+} spikes that we observe in CSFcNs are able to evoke synaptic release, with the HVA channels providing higher rates of vesicle release or possibly multivesicular release. Such dual modes of release have been described in chick auditory hair cells where T-type Ca^{2+}currents regulate rapid vesicle release and L-type Ca^{2+} channels regulate sustained neurotransmitter release (Levic and Dulon, 2012).

The ventral and dorsolateral CSFcNs have different developmental origins (Petracca et al., 2016; Djenoune et al., 2017) and in zebrafish this gives rise to different functional types with corresponding projections. Ventral CSFcNs respond to longitudinal spinal contractions, project to fast motor neurons and are required for correct escape behaviours (Hubbard et al., 2016), whereas dorsal CSFcNs are activated by tail bends and regulate spontaneous locomotion by interacting with the central pattern generator (Böhm et al., 2016). Such functional insights are yet to be gained in the mammalian spinal cord. Our data indicate that there is no dorsoventral difference between the presence of spontaneous activity nor in the expression of ACh receptors, as all cells were responsive. Functional P2 receptor expression did however correlate with the dorsoventral positioning of CSFcNs around the central canal. UTP-responsive CSFcNs, likely expressing P2Y receptors, were clustered in lateral aspects of the central canal, whilst $P2X_3$ receptors were restricted to ventral CSFcNs. It remains to be determined whether distinct functional types of CSFcNs exist in the mammalian spinal cord and whether these are spatially organised.

Despite the cell-cell variability in functional P2 receptor expression, all purinergic evoked responses were T-type Ca^{2+} channel dependent and this included the metabotropic P2Y responses. The mechanism of coupling between P2Y receptor activation and generation of T-type Ca^{2+} spikes is not yet clear. This could occur through direct activation of the T-type Ca^{2+} as has been observed with mGluR receptors in olfactory bulb neurons (Johnston and Delaney, 2010). Alternatively P2Y receptors may evoke hyperpolarisation which then generates T-type dependent rebound spiking as has been for dopaminergic (Evans et al., 2017) and GABAergic

receptors (Leresche and Lambert, 2018). The ATP responses with initial decreases in Ca^{2+} (Fig. 7 G) indicate that this may be the possible explanation.

In conclusion, we provide novel evidence that CSFcNs use T-type Ca^{2+} channels to generate spontaneous activity and also to respond to low amplitude inputs. We reveal how CSFcNs use graded Ca^{2+} spikes to respond to inputs from different neurotransmitter systems via distinct mechanisms. These observations closely mirror findings within other sensory systems and are consistent with CSFcNs functioning as a multi-modal chemosensory neuron within the mammalian spinal cord. By successfully characterising CSFcN signalling within adult mouse spinal CSFcNs we assert the utility of transgenic lines to further investigate the projection pathways and their potential role in spinal output.

Methods

Animal handling and experimentation was carried out according to UK Home Office guidelines and the requirements of the United Kingdom Animals (Scientific Procedures) Act 1986. Mice were housed under a 12:12 h light/dark cycle with free access to food and water. All efforts were made to minimize animal suffering and the number of animals used. Vesicular GABA transporter-IRES-Cre mice (*VGAT.Cre*, stock 028862, B6J.129S6(FVB)-Slc32a1<tm2(cre)) were crossed with floxed GCaMP6f mice (*GCaMP6f.flox,* stock 028865, B6J.CgGt(ROSA)26Sor<tm95.1 (CAGGCaMP6f)), to generate VGATxGCaMP6f mice. Both mouse lines were originally from Jackson Laboratory (Maine, USA) and maintained in house. All chemicals and drugs were purchased from Sigma-Aldrich (Gillingham, UK) unless otherwise stated.

Immunohistochemistry (IHC). Adult VGATxGCamP6f mice (P30-P52) were anaesthetised with a terminal dose of sodium pentobarbital (100mg.kg-^{1}, I.P, Euthatal, Merial Animal Health, Dublin) and transcardially perfused, initially with phosphate buffer (PB, 0.1M) to remove blood, and then with paraformaldehyde (PFA, 4% in 0.1M PB, 250ml). Brains and spinal cords were removed and post-fixed overnight in PFA. Spinal cords were serially sectioned (40µm, VT1200 vibrating microtome, Leica Microsystems, Milton Keynes, UK) and stored in PBS at 4ºC. Sections were incubated with anti-PKD2L1 (1:500, rabbit, Proteintech) and anti-GFP (1:1000, chicken, Abcam) dissolved in PBS with 0.2% Triton X-100 with 5% donkey serum as a non-specific binding blocker. Sections were washed (x3, PBS 10 minutes) before addition of the Alexa Fluor conjugated secondary antibody (1:1000 in PBS, Thermofisher) at room temperature for 2h. Sections were washed (x2 PBS, 10 minutes) before being mounted on microscope slides and allowed to air dry. Sections were covered using vectashield with DAPI (VectorLabs, cat no. H-1800) and a coverslip was added and sealed using nail varnish.

Acute slice preparation. VGATxGCamP6f mice (P14-P55, both sexes) were terminally anaesthetised with sodium pentobarbital (as above) and decapitated. The spinal column was dissected and spinal cords were hydraulically extruded via pressure ejection of oxygenated (95% O_2 : 5% CO_2) sucrose artificial cerebrospinal fluid (sACSF, 30°C, 26mM $NaHCO_3$, 2.5mM NaH_2PO_4, 3mM KCl, 217mM sucrose, 10mM glucose, 2mM $MgSO_4.7H_20$, 1mM $CaCl_2$) through the caudal end of the spinal canal, via a 25ml syringe. Thoracolumbar SC was embedded in agar (1.5% in sACSF) and sectioned transversely using a vibrating microtome (400µm, Integraslice 7550, Campden Instruments, Loughborough, UK), in sACSF (30°C). Spinal cord sections were transferred to a submerged incubation chamber containing standard ACSF (124mM NaCl, 26mM $NaHCO_3$, 10mM glucose, 3mM KCl, 2.5mM NaH_2PO_4, 2mM $MgSO_4.7H_20$, 2mM $CaCl_2$, room temp), for ≥1 hour prior to recording.

2-photon Ca^{2+} imaging. Spinal cord slices were transferred to the recording chamber, of a custom built 2-P laser scanning microscope, and perfused with oxygenated ACSF (room temp, 20ml/min), driven by a peristaltic pump. GCaMP6f fluorescence was excited at 910 nm using a pulsed Mai Tai eHP DeepSee Ti:sapphire laser system (SpectraPhysics, Santa Clara, CA, USA). A resonant-galvo mirror assembly (Sutter instruments, UK) scanned the beam through a 16x water-dipping objective (N16XLWD-PF, NA 0.8, Nikon, Tokyo, Japan). Fluorescence was detected using GAasP photomultiplier tubes and appropriate filters and dichroic mirrors. Images were acquired at 30Hz, using ScanImage v.5 software (Pologruto et al., 2003). To study evoked Ca^{2+} activity, drugs were loaded into microinjection patch electrodes (3-4µm tip diameter) held via an electrode holder controlled by a MP285 micromanipulator (Sutter Instruments, USA), and connected to a picospritzer II (Parker, USA). Sulforhodamine 101 (SR101, 12.5M) was included in the pipette solution to confirm successful drug application.

Data analysis. *Spontaneous Ca^{2+} event analysis* – The batch processing pipeline of CaImAn was used to correct any motion artefacts and segment cells (Giovannucci et al., 2019). Due to the irregular shape of CSFcNs we did not use the CNN classifier. Subsequent analysis of the segmented cells' time series was performed in Igor Pro (wavemetrics). Time series were first filtered with a 4th order Saviztky-Golay filter with a 9 point window. Spikes were then detected using the first derivative with the threshold set manually for each slice. Spike amplitudes were measured as the difference between the peak $\Delta F/F$ signal occurring in a 333ms window around the spike time and the mean signal in the preceding 166ms (Blue arrows in Fig. 2C). The Jarque-Bera statistic was used to assess multi-modality in the spike amplitudes of individual cells (Fig. 2I).

Evoked Ca^{2+} event analysis – As focal drug application elicited rapid Ca^{2+} increases in multiple CSFcNs simultaneously, automated segmentation underestimated the number of CSFcNs. These data were therefore manually analysed using FIJI (Schindelin at al., 2012). ROIs were drawn around individual CSFcNs and fluorescence intensity measured, background

fluorescence measured from non-GCaMP6f expressing areas was removed and signals normalised (ΔF/F). Average amplitudes from 3 focal applications were taken.

All data are expressed as mean ± SEM unless otherwise stated and all statistical analyses were performed using GraphPad Prism version 8 (GraphPad Software, Inc).

References

BADEN, T., BERENS, P., BETHGE, M. & EULER, T. 2013. Spikes in mammalian bipolar cells support temporal layering of the inner retina. *Curr Biol,* 23**,** 48-52.

BADEN, T., ESPOSTI, F., NIKOLAEV, A. & LAGNADO, L. 2011. Spikes in retinal bipolar cells phase-lock to visual stimuli with millisecond precision. *Curr Biol,* 21**,** 1859-69.

BOEHME, R., UEBELE, V. N., RENGER, J. J. & PEDROARENA, C. 2011. Rebound excitation triggered by synaptic inhibition in cerebellar nuclear neurons is suppressed by selective T-type calcium channel block. *J Neurophysiol,* 106**,** 2653-61.

BOHM, U. L., PRENDERGAST, A., DJENOUNE, L., NUNES FIGUEIREDO, S., GOMEZ, J., STOKES, C., KAISER, S., SUSTER, M., KAWAKAMI, K., CHARPENTIER, M., CONCORDET, J. P., RIO, J. P., DEL BENE, F. & WYART, C. 2016. CSF-contacting neurons regulate locomotion by relaying mechanical stimuli to spinal circuits. *Nat Commun,* 7**,** 10866.

BRANDT, A., STRIESSNIG, J. & MOSER, T. 2003. CaV1.3 channels are essential for development and presynaptic activity of cochlear inner hair cells. *J Neurosci,* 23**,** 10832-40.

COMUNANZA, V., MARCANTONI, A., VANDAEL, D. H., MAHAPATRA, S., GAVELLO, D., CARABELLI, V. & CARBONE, E. 2010. CaV1.3 as pacemaker channels in adrenal chromaffin cells: specific role on exo- and endocytosis? *Channels (Austin),* 4**,** 440-6.

CORNS, L. F., ATKINSON, L., DANIEL, J., EDWARDS, I. J., NEW, L., DEUCHARS, J. & DEUCHARS, S. A. 2015. Cholinergic Enhancement of Cell Proliferation in the Postnatal Neurogenic Niche of the Mammalian Spinal Cord. *Stem Cells,* 33**,** 2864-76.

DJENOUNE, L., KHABOU, H., JOUBERT, F., QUAN, F. B., NUNES FIGUEIREDO, S., BODINEAU, L., DEL BENE, F., BURCKLE, C., TOSTIVINT, H. & WYART, C. 2014. Investigation of spinal cerebrospinal fluid-contacting neurons expressing PKD2L1: evidence for a conserved system from fish to primates. *Front Neuroanat,* 8**,** 26.

DREOSTI, E., ESPOSTI, F., BADEN, T. & LAGNADO, L. 2011. In vivo evidence that retinal bipolar cells generate spikes modulated by light. *Nat Neurosci,* 14**,** 951-2.

EVANS, R. C., ZHU, M. & KHALIQ, Z. M. 2017. Dopamine Inhibition Differentially Controls Excitability of Substantia Nigra Dopamine Neuron Subpopulations through T-Type Calcium Channels. *J Neurosci,* 37**,** 3704-3720.

FIDELIN, K., DJENOUNE, L., STOKES, C., PRENDERGAST, A., GOMEZ, J., BARADEL, A., DEL BENE, F. & WYART, C. 2015. State-Dependent Modulation of Locomotion by GABAergic Spinal Sensory Neurons. *Curr Biol,* 25**,** 3035-47.

GIOVANNUCCI, A., FRIEDRICH, J., GUNN, P., KALFON, J., BROWN, B. L., KOAY, S. A., TAXIDIS, J., NAJAFI, F., GAUTHIER, J. L., ZHOU, P., KHAKH, B. S., TANK, D. W., CHKLOVSKII, D. B. & PNEVMATIKAKIS, E. A. 2019. CaImAn an open source tool for scalable calcium imaging data analysis. *Elife,* 8.

GOLDING, N. L., JUNG, H. Y., MICKUS, T. & SPRUSTON, N. 1999. Dendritic calcium spike initiation and repolarization are controlled by distinct potassium channel subtypes in CA1 pyramidal neurons. *J Neurosci,* 19**,** 8789-98.

HU, C., BI, A. & PAN, Z. H. 2009. Differential expression of three T-type calcium channels in retinal bipolar cells in rats. *Vis Neurosci,* 26**,** 177-87.

HUANG, A. L., CHEN, X., HOON, M. A., CHANDRASHEKAR, J., GUO, W., TRANKNER, D., RYBA, N. J. & ZUKER, C. S. 2006. The cells and logic for mammalian sour taste detection. *Nature,* 442**,** 934-8.

HUANG, L. Y. 1989. Calcium channels in isolated rat dorsal horn neurones, including labelled spinothalamic and trigeminothalamic cells. *J Physiol,* 411**,** 161-77.

HUBBARD, J. M., BOHM, U. L., PRENDERGAST, A., TSENG, P. B., NEWMAN, M., STOKES, C. & WYART, C. 2016. Intraspinal Sensory Neurons Provide Powerful Inhibition to Motor Circuits Ensuring Postural Control during Locomotion. *Curr Biol,* 26**,** 2841-2853.

HUMPHREY, T. 1947. Sensory ganglion cells within the central canal of the embryonic human spinal cord. *J Comp Neurol,* 86**,** 1-35.

JACOBSON, K. A., IVANOV, A. A., DE CASTRO, S., HARDEN, T. K. & KO, H. 2009. Development of selective agonists and antagonists of P2Y receptors. *Purinergic Signal,* 5**,** 75-89.

JALALVAND, E., ROBERTSON, B., TOSTIVINT, H., LOW, P., WALLEN, P. & GRILLNER, S. 2018. Cerebrospinal Fluid-Contacting Neurons Sense pH Changes and Motion in the Hypothalamus. *J Neurosci,* 38**,** 7713-7724.

JALALVAND, E., ROBERTSON, B., TOSTIVINT, H., WALLEN, P. & GRILLNER, S. 2016a. The Spinal Cord Has an Intrinsic System for the Control of pH. *Curr Biol,* 26**,** 1346-51.

JALALVAND, E., ROBERTSON, B., WALLEN, P. & GRILLNER, S. 2016b. Ciliated neurons lining the central canal sense both fluid movement and pH through ASIC3. *Nat Commun,* 7**,** 10002.

JALALVAND, E., ROBERTSON, B., WALLEN, P., HILL, R. H. & GRILLNER, S. 2014. Laterally projecting cerebrospinal fluid-contacting cells in the lamprey spinal cord are of two distinct types. *J Comp Neurol,* 522**,** Spc1.

JOHNSON, S. L., ECKRICH, T., KUHN, S., ZAMPINI, V., FRANZ, C., RANATUNGA, K. M., ROBERTS, T. P., MASETTO, S., KNIPPER, M., KROS, C. J. & MARCOTTI, W. 2011. Position-dependent patterning of spontaneous action potentials in immature cochlear inner hair cells. *Nat Neurosci,* 14**,** 711-7.

JOHNSTON, J. & DELANEY, K. R. 2010. Synaptic activation of T-type Ca2+ channels via mGluR activation in the primary dendrite of mitral cells. *J Neurophysiol,* 103**,** 2557-69.

JOINER, M. L. & LEE, A. 2015. Voltage-Gated Cav1 Channels in Disorders of Vision and Hearing. *Curr Mol Pharmacol,* 8**,** 143-8.

KOLMER, W. 1921. Das „Sagittalorgan“ der Wirbeltiere. *Zeitschrift für Anatomie und Entwicklungsgeschichte,* 60**,** 652-717.

LATTANZI, D., DI PALMA, M., CUPPINI, R. & AMBROGINI, P. 2020. GABAergic Input Affects Intracellular Calcium Levels in Developing Granule Cells of Adult Rat Hippocampus. *Int J Mol Sci,* 21.

LEE, C. H. & RUBEN, P. C. 2008. Interaction between voltage-gated sodium channels and the neurotoxin, tetrodotoxin. *Channels (Austin),* 2**,** 407-12.

LERESCHE, N. & LAMBERT, R. C. 2018. GABA receptors and T-type Ca(2+) channels crosstalk in thalamic networks. *Neuropharmacology,* 136**,** 37-45.

LEVIC, S. & DULON, D. 2012. The temporal characteristics of Ca2+ entry through L-type and T-type Ca2+ channels shape exocytosis efficiency in chick auditory hair cells during development. *J Neurophysiol,* 108**,** 3116-23.

LIPIN, M. Y. & VIGH, J. 2015. Calcium spike-mediated digital signaling increases glutamate output at the visual threshold of retinal bipolar cells. *J Neurophysiol,* 113**,** 550-66.

LY, R., BOUVIER, G., SZAPIRO, G., PROSSER, H. M., RANDALL, A. D., KANO, M., SAKIMURA, K., ISOPE, P., BARBOUR, B. & FELTZ, A. 2016. Contribution of postsynaptic T-type calcium channels to parallel fibre-Purkinje cell synaptic responses. *J Physiol,* 594**,** 915-36.

MA, Y. P. & PAN, Z. H. 2003. Spontaneous regenerative activity in mammalian retinal bipolar cells: roles of multiple subtypes of voltage-dependent Ca2+ channels. *Vis Neurosci,* 20**,** 131-9.

MAJOR, G., LARKUM, M. E. & SCHILLER, J. 2013. Active properties of neocortical pyramidal neuron dendrites. *Annu Rev Neurosci,* 36**,** 1-24.

MARCOTTI, W., JOHNSON, S. L., RUSCH, A. & KROS, C. J. 2003. Sodium and calcium currents shape action potentials in immature mouse inner hair cells. *J Physiol,* 552**,** 743-61.

MLINAR, B., BIAGI, B. A. & ENYEART, J. J. 1993. Voltage-gated transient currents in bovine adrenal fasciculata cells. I. T-type Ca2+ current. *J Gen Physiol,* 102**,** 217-37.

RAGHAVAN, M., FEE, D. & BARKHAUS, P. E. 2019. Generation and propagation of the action potential. *Handb Clin Neurol,* 160**,** 3-22.

ROSENBERG, A. B., ROCO, C. M., MUSCAT, R. A., KUCHINA, A., SAMPLE, P., YAO, Z., GRAYBUCK, L. T., PEELER, D. J., MUKHERJEE, S., CHEN, W., PUN, S. H., SELLERS, D. L., TASIC, B. & SEELIG, G. 2018. Single-cell profiling of the developing mouse brain and spinal cord with split-pool barcoding. *Science,* 360**,** 176-182.

SCHRIER, A. D., WANG, H., TALLEY, E. M., PEREZ-REYES, E. & BARRETT, P. Q. 2001. alpha1H T-type Ca2+ channel is the predominant subtype expressed in bovine and rat zona glomerulosa. *Am J Physiol Cell Physiol,* 280**,** C265-72.

STERNBERG, J. R., PRENDERGAST, A. E., BROSSE, L., CANTAUT-BELARIF, Y., THOUVENIN, O., ORTS-DEL'IMMAGINE, A., CASTILLO, L., DJENOUNE, L., KURISU, S., MCDEARMID, J. R., BARDET, P. L., BOCCARA, C., OKAMOTO, H., DELMAS, P. & WYART, C. 2018. Pkd2l1 is required for mechanoception in cerebrospinal fluid-contacting neurons and maintenance of spine curvature. *Nat Commun,* 9**,** 3804.

STOECKEL, M. E., UHL-BRONNER, S., HUGEL, S., VEINANTE, P., KLEIN, M. J., MUTTERER, J., FREUND-MERCIER, M. J. & SCHLICHTER, R. 2003. Cerebrospinal fluid-contacting neurons in the rat spinal cord, a gamma-aminobutyric acidergic system expressing the P2X2 subunit of purinergic receptors, PSA-NCAM, and GAP-43 immunoreactivities: light and electron microscopic study. *J Comp Neurol,* 457**,** 159-74.

TOMIC, M., KOSHIMIZU, T., YUAN, D., ANDRIC, S. A., ZIVADINOVIC, D. & STOJILKOVIC, S. S. 1999. Characterization of a plasma membrane calcium oscillator in rat pituitary somatotrophs. *J Biol Chem,* 274**,** 35693-702.

TRAN-VAN-MINH, A., ABRAHAMSSON, T., CATHALA, L. & DIGREGORIO, D. A. 2016. Differential Dendritic Integration of Synaptic Potentials and Calcium in Cerebellar Interneurons. *Neuron,* 91**,** 837-850.

WANG, J., OU, S. W. & WANG, Y. J. 2017. Distribution and function of voltage-gated sodium channels in the nervous system. *Channels (Austin),* 11**,** 534-554.

WYART, C., DEL BENE, F., WARP, E., SCOTT, E. K., TRAUNER, D., BAIER, H. & ISACOFF, E. Y. 2009. Optogenetic dissection of a behavioural module in the vertebrate spinal cord. *Nature,* 461**,** 407-10.

XU, N. L., HARNETT, M. T., WILLIAMS, S. R., HUBER, D., O'CONNOR, D. H., SVOBODA, K. & MAGEE, J. C. 2012. Nonlinear dendritic integration of sensory and motor input during an active sensing task. *Nature,* 492**,** 247-51.

ZAMPINI, V., JOHNSON, S. L., FRANZ, C., LAWRENCE, N. D., MUNKNER, S., ENGEL, J., KNIPPER, M., MAGISTRETTI, J., MASETTO, S. & MARCOTTI, W. 2010. Elementary properties of CaV1.3 Ca(2+) channels expressed in mouse cochlear inner hair cells. *J Physiol,* 588**,** 187-99.